FE Implementation of AA6xxx Series Aluminium Pre-strain Dependent Strengthening Response During Paint Bake

Sebastijan Jurendic[1], Richard Burrows[2], Shuvra Saha[3], Zeqin Liang[1]

[1]Novelis Deutschland GmbH
[2]Novelis Global R&D Centre
[3]RWTH Aachen, IBF

1 Introduction

Heat treatable aluminium alloys have several advantages over non heat treatable alloys in automotive production. Not least of these is the ability to be formed in a soft and ductile state while being strengthened later on in the production process using heat treatment to achieve a high strength component. In numerical simulation of automotive structures this can pose a challenge as the change of material properties during the heat treatment depends on several factors, one of which is the amount of strain the material is subjected to during forming. As parts of arbitrary shapes in general end up with a non-uniform stress-strain distribution after forming, it stands to reason that the material strength after heat treatment will be non-uniform across the part as well. Knowing the material strength distribution within a part and applying it to finite element simulations could potentially improve the predictive capability of crash analysis of automotive structures leading to a higher level of optimization and ultimately reducing the weight of a vehicle.
In this work a microstructural evolution model for 6xxx heat treatable aluminium alloys, taking into account the effects of pre-strain as well as heat treatment parameters, is presented. The model is validated for a representative 6xxx series alloy against tensile test data and a cylindrical deep draw process. A simple implementation of the pre-strain dependent strengthening response into a finite element model is carried out using measured data and demonstrated on an example of axially crushing a formed tube.

2 Application of 6xxx series rolled aluminium alloys in the automotive industry

6xxx series aluminium alloys consist of Si, Mg and sometimes Cu as the main alloying elements and belong to the family of heat treatable alloys. A typical automotive age-hardenable sheet material is produced by hot and cold rolling and is finished by annealing at an elevated temperature (~540-570 °C) before it is shipped to the automotive manufacturer [1]. The final annealing process, also called solutionizing heat treatment, has two major purposes: 1) to achieve full recovery and recrystallization of the microstructure, which maximizes the formability in the automotive manufacturing process (stamping, bending and hemming); 2) to dissolve the soluble alloying elements into solid solution so that they can form precipitates later on. The precipitates, namely beta" and beta', form during heating in the paint bake process and they provide the strengthening which leads to the high material strength in the finished component. The process route in automotive production is illustrated in Fig.1.

(a) (b) (c)

Fig.1: final process route of 6xxx series aluminium alloys: (a) final annealing (b) forming (c) paint bake treatment.

3 Modelling of the final strength by considering microstructural evolution during the process route

Although the sheet which is shipped to the automotive manufacturer has relatively uniform mechanical properties, the final strength of the 6xxx alloy is influenced by the amount of cold work experienced, the stress relaxation during the paint bake treatment and the hardening contribution of the newly formed precipitates. When all the contributions from the microstructure are considered, the final yield stress σ_{total} of the alloy is given as [2]:

$$\sigma_{total} = \sigma_{Al} + \sigma_{gb} + M(\tau_d + \tau_{ss}) + \sigma_{ppt}. \quad (1)$$

Where σ_{Al} is the intrinsic strength of the aluminium matrix, σ_{gb} is the strengthening contribution of the grain boundaries, M the Taylor factor, τ_d critical resolved shear stress due to stored dislocations caused by deformation, τ_{ss} is the contribution of solid solution strengthening and σ_{ppt} is the strengthening contribution from the hardening precipitates.
In this case, σ_{Al} and σ_{gb} can be treated as constants during the application. The complexity comes as the formation of the precipitates is also influenced by the strain level as it introduces a different amount of dislocations, which help to accelerate the nucleation and growth of the precipitates. If we consider the precipitates which form along the dislocations, the stress contribution from the precipitation is given as:

$$\sigma_{ppt} = \sigma_{ppt}^{dis}(T,t) + \sigma_{ppt}^{matrix}(T,t). \quad (2)$$

Where $\sigma_{ppt}^{dis}(T,t)$ is the strengthening contribution from the formation of precipitates along dislocations caused by the deformation and $\sigma_{ppt}^{matrix}(T,t)$ the strengthening contribution from the formation of precipitates in the matrix. It should be noted that the amount of dislocations also changes during the paint bake treatment, appearing as stress relaxation, which in itself dynamically influences the formation of precipitates along the dislocations as well. Moreover, τ_{ss} changes due to the change in solute content in the matrix as it is used up in the formation of the precipitates.
When all the contributions from the microstructure need to be considered, mapping the final strength of the sheet after forming and paint bake becomes challenging both experimentally as well as using simulation. In order to tackle this challenge, a microstructural model taking into account the level of deformation, precipitation formation and stress relaxation to predict the final strength [3] is used in conjunction with finite element simulation.
Fig. 2 shows the strength evolution during paint bake treatment at a temperature of 185 °C as a function of time with different levels of pre-strain: 0, 5 and 10 % respectively. The part with no strain has the slowest increase of the yield strength during paint bake treatment, as shown in Fig. 2 (a). Compared with 5 % strain, the part with 10 % strain has a higher strength contributed of the stored dislocations due to higher strain while the kinetics of the precipitation hardening are accelerated (see Fig. 2 (b) and (c)). It is also noted that the part with the highest strain (10 %) also achieves the highest strength with a value of approximately 275 MPa.

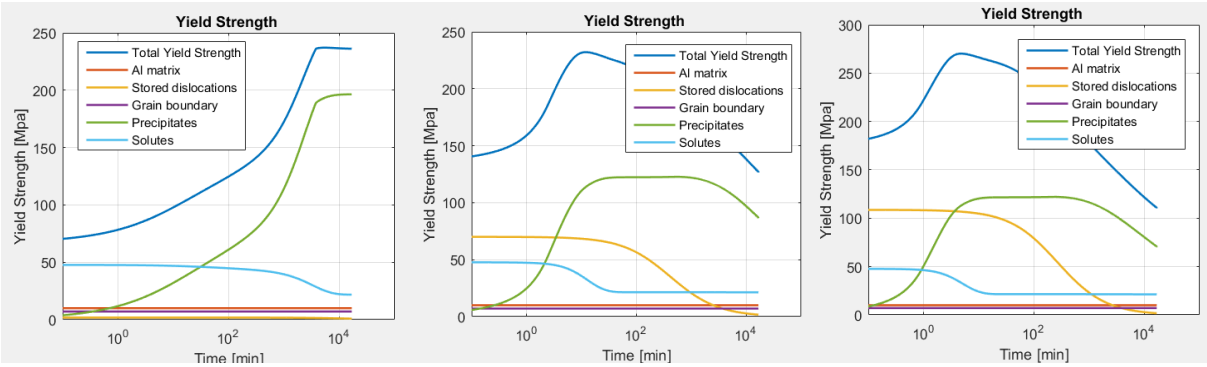

Fig.2: strength evolution of a 6xxx series alloy during paint bake treatment at 185 °C after a pre-strain of a) 0% b) 5 % and c) 10 %

4 Validation of the yield strength prediction model

Only the initial yield strength of the material can be predicted by the microstructural model in its current state. Two types of tests were carried out to validate the predictions: tensile tests and a cylindrical cup draw. The reason for this is that the maximum pre-strain achievable in tensile testing is limited by the onset of necking, to circumvent this issue, the cup draw test was introduced as a means of obtaining higher strains. Since determining the strains during a deep draw operation was not possible directly, the physical test needed to be augmented by a finite element analysis to provide this information.
The material used in this investigation was a 6xxx series alloy sheet of 1.15 mm thickness, representative of a typical heat treatable alloy found in automotive production.

4.1 Tensile testing

Tensile tests were carried out to determine the mechanical properties of the material, both for microstructural model validation and to provide input data for FEA. To evaluate the different levels of pre-strain the work flow was as follows:

1. Solutionizing
2. Pre-straining
3. Paint bake simulation
4. Final testing

The solutionizing was performed by annealing the material at 550 °C for 30 min and quenching in water. This represents the material as it would enter the forming process. To limit the effect of natural ageing, the pre-straining was performed directly after solutionizing in a consistent and timely manner.
Pre-straining was performed using a standard tensile testing frame by axially straining the samples until the desired level of elongation was achieved. The ISO 6892-1:2009 international standard [4] was followed as closely as practically possible. The pre-strain levels considered in this work are: unstrained, 2%, 4%, 8% and 12%. Higher pre-strains could not be achieved due to the onset of necking. For each pre-strain condition five repeat samples were tested.
Age hardening has been carried out in such a way as to represent the paint bake process in automobile production. The previously pre-strained samples were exposed to 185 °C for 20 min and then rapidly cooled to achieve consistency.
In final testing, the age hardened samples were tested up to failure using the same conditions as during pre-straining. Fig. 3 shows the measured engineering stress-strain curves for the different pre-strain levels. One representative curve from each set has been selected for plotting to make the figure easier to read.

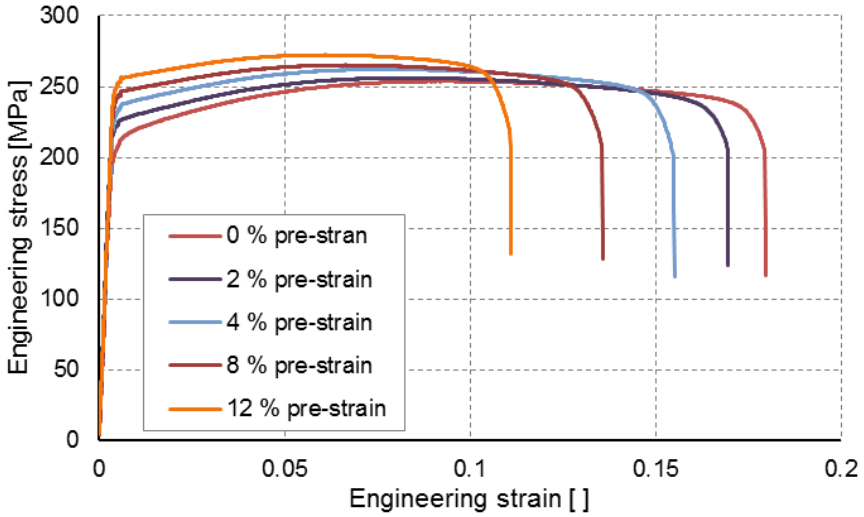

Fig.3: representative engineering stress-strain curves after paint bake for different levels of pre-strain.

The measured response displayed on Fig. 3 clearly illustrates the effect of increasing pre-strain on the material properties after paint-bake. The yield point increases significantly from approximately 205 MPa to approximately 255 MPa while at the same time the elongation to break drastically reduces from approximately 18 % to about 11 %.

The increase in yield stress is more clearly shown on Fig. 4, which also includes the standard deviation of the measurement.

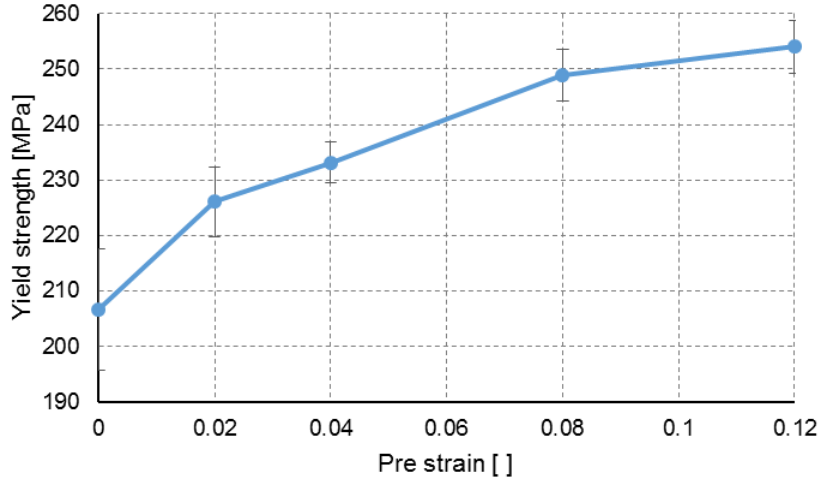

Fig.4: yield strength after paint bake as a function of pre-strain.

The measurement scatter is perhaps larger than usually experienced in standard tensile testing, which could be a consequence of inconsistencies in the heat treatment process.

4.2 Cup draw and hardness test

In order to evaluate the age hardening effect at higher strains, a cup draw test was performed to provide the pre-straining deformation. Measurement of mechanical properties was performed by sectioning the drawn cups and performing a Vickers hardness test, the measured hardness values were then later converted to approximate tensile yield stress equivalents using a linear relationship:

$$\sigma_Y = 3.222\,HV - 2.963 \tag{3}$$

The workflow was similar as with the tensile test, where pre-straining was replaced by the cup draw process and the final testing by the Vickers hardness test. Before drawing, the material was solution heat treated in the same manner as with the tensile test. The drawing process was performed using cups of 33 mm internal diameter drawn from 60 mm circular blanks. The test tooling geometry is shown on Fig. 5 (a).
The drawn cups were subjected to the paint bake simulation consisting of the same heat treatment as with the tensile test samples. Heat-treated cups were then sectioned along the middle plane and Vickers hardness measurements were performed on the exposed surface, measured values were averaged according to symmetry. The indentations were performed along the middle line of the cup sidewall at pre-defined positions from the centre and the top of the cup (Fig. 5 (b)).

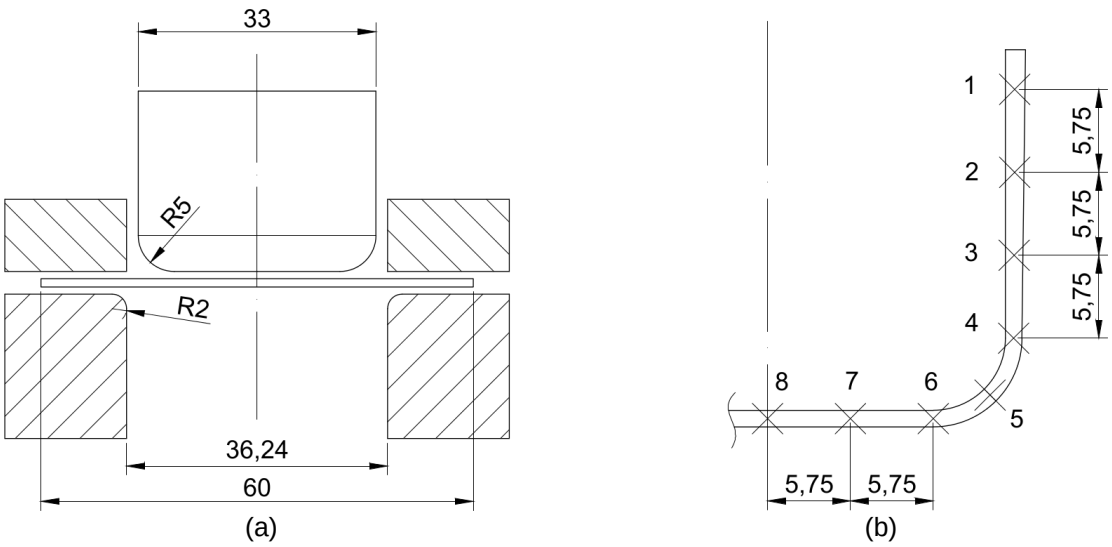

Fig.5: a) cup draw tooling geometry and b) Vickers hardness measurement points.

The measured cup sidewall hardness profile is shown on Fig. 6.

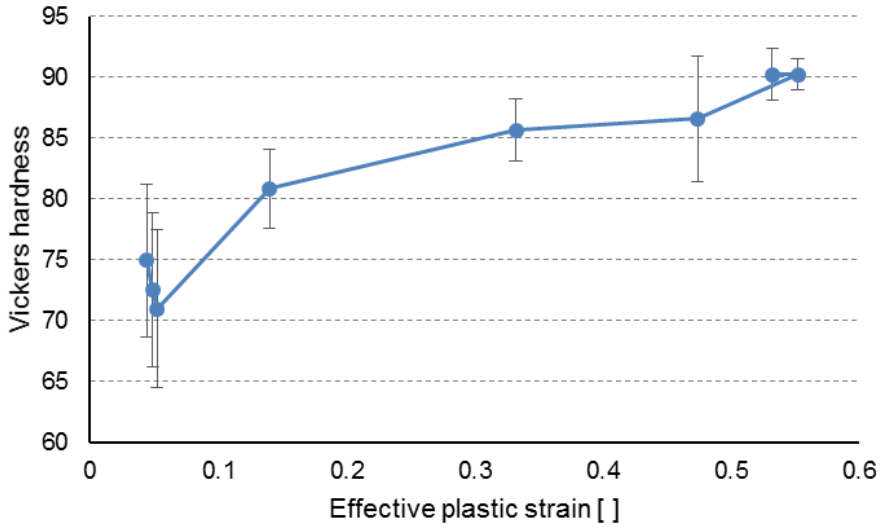

Fig.6: measured hardness profile along the cup wall cross-section.

4.2.1 Determining cup pre-strain

To establish the correlation between pre-strain and age-hardening level, the amount of deformation during the cupping test needs to be determined. A finite element model of the cup draw process was developed to this effect, as shown on Fig. 7.

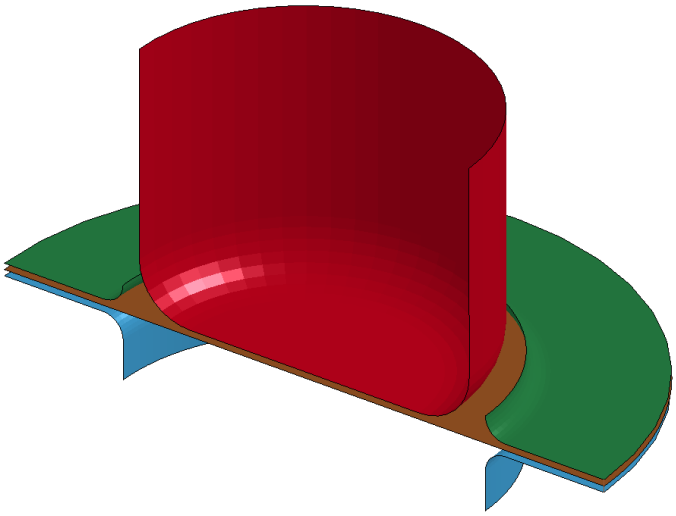

Fig.7: cup draw finite element model.

The model consists of three rigid tools modelled by shell elements and a deformable blank, also modelled using shells. A rigid body stopper is used to prevent the blank holder form falling through the draw die after the blank has been fully drawn. The blank uses an isotropic elasto-plastic material model, with the material properties determined from tensile test data. The hardening behaviour is described using a load curve, high strain extrapolation is handled by using the Voce equation.
Strains at points corresponding to the Vickers hardness measurements on the actual cup were evaluated at the midplane of the shell elements, which is also consistent with the physical measurement. The effective plastic strains achieved at various positions along the cup are shown on Fig. 8.

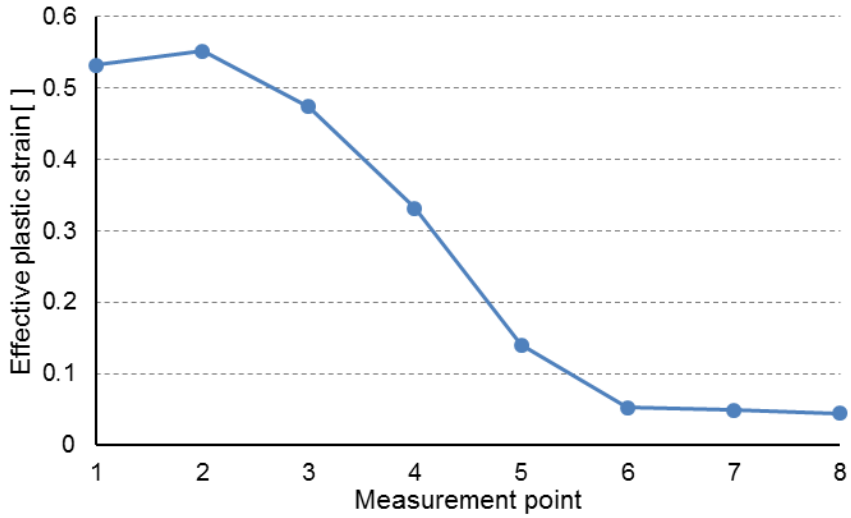

Fig.8: effective plastic strain on the shell midplane at different points along the cup sidewall.

4.3 Model predictions vs. measured data

Fig. 9 shows the model prediction and experimentally determined yield strength after the paint bake heat treatment of 185 °C for 20 min as a function of pre-strain level. There is an initial offset in the model predictions around 0 % pre-strain, that is a consequence of the model calibration for the particular alloy considered here. Past the initial discrepancy, the model describes the increase of the yield strength reasonably well, capturing both the initial steep strengthening response as well as the yield saturation at higher pre-strains.

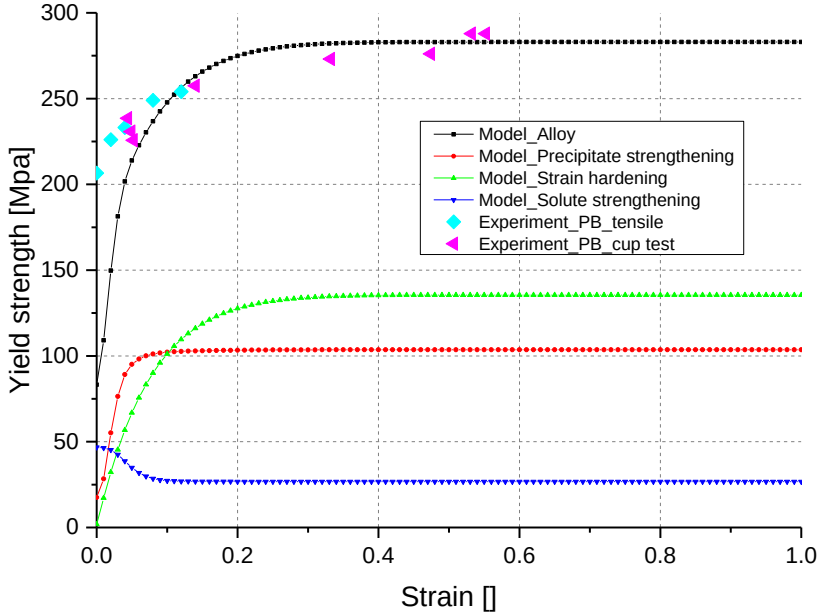

Fig.9: model validation by tensile and cup test.

The model indicates that the initial increase consists of both strain hardening and the promotion of precipitation hardening effect due to pre-strain, whilst the solute strengthening decreased as more solutes participated in the precipitate formation. The precipitation hardening effects saturates at relatively low levels of pre-strain, approximately 10 % after which point the main strengthening effect comes from strain hardening.

5 Finite element simulation

To evaluate the magnitude of influence that the pre-strain dependent paint bake response has on an actual part in crash-like simulation conditions, a multi-step simulation of a quasi-static tube crush

scenario was created. The tube itself consists of a channel that is deep-drawn from a flat piece of sheet and a panel that is riveted to its bottom. The geometry of the tube can be seen on Fig. 10, the dimensions were omitted due to the test being proprietary. Crosses on the figure represent riveting points.

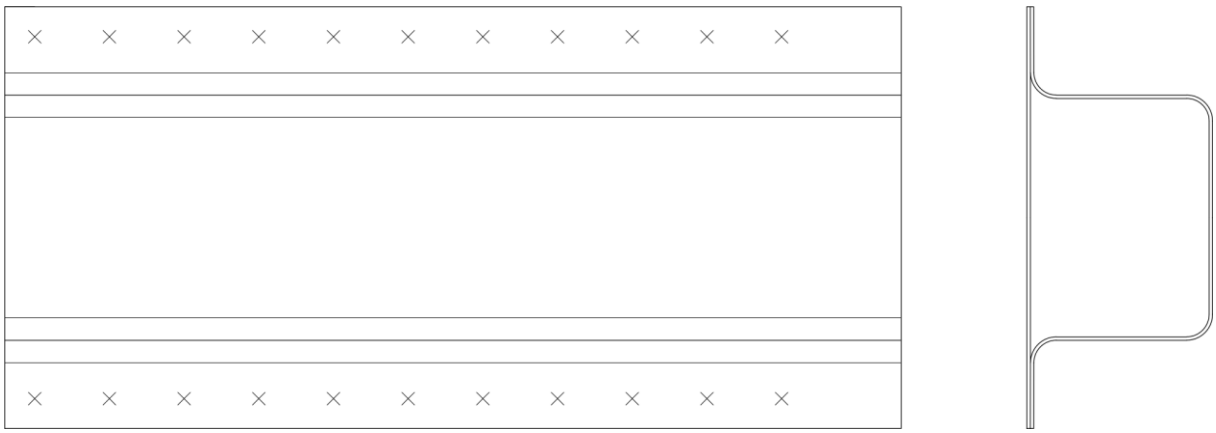

Fig.10: tube geometry.

5.1 Pre-strain dependent age hardening implementation

In its current form, the implementation of pre-strain dependent paint-bake response is somewhat simplified. After a forming simulation step the effective plastic strains for each element are averaged across all integration points and stored in a history variable. Based on that value, the elasto-plastic material model uses a lookup table containing hardening curves at different pre-strain levels to establish the stress-strain response of any particular element using linear interpolation. Between the forming and subsequent steps in the simulation workflow, the materials strain hardening properties are substituted from those in the solutionized conditions by the final pre-strain dependent strain-stress response, simulating the microstructural transformation.
This approach has the distinct disadvantage that the through thickness strain distribution is not taken into account, thus inaccuracies around tight radii are expected.
The 3D surface formed by the yield stress as a function of pre-strain and instantaneous effective plastic strain for the material in this investigation is shown on Fig. 11. This is a direct input for the post-paint-bake material model.

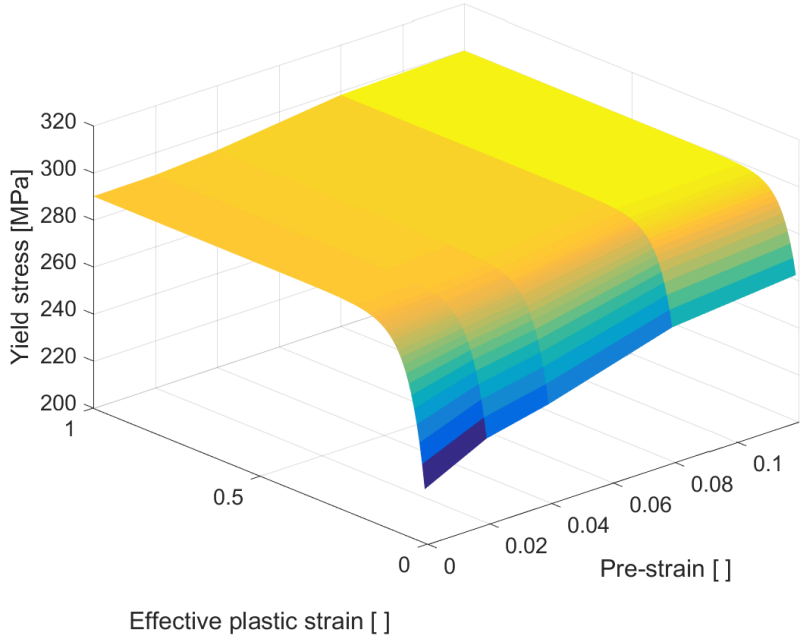

Fig.11: yield stress as a function of pre-strain and effective plastic strain.

5.2 Simulation procedure

The simulation sequence consists of three stages:

1. Channel draw
2. Springback and riveting
3. Axial crush

The channel is drawn in a deep-drawing like process. After the drawing simulation the bottom plate is attached using pre-loaded discrete beam elements to simulate the rivets. The elements used in the simulation were fully integrated thin shell elements, the channel and plate are meshed with a uniform mesh of 2x2 mm square elements. In between the draw and the springback stages, the material hardening properties are changed from the as-solutionized to the after paint-bake properties and a dynamic springback step is executed. The pre-strain after springback is shown on Fig. 12.

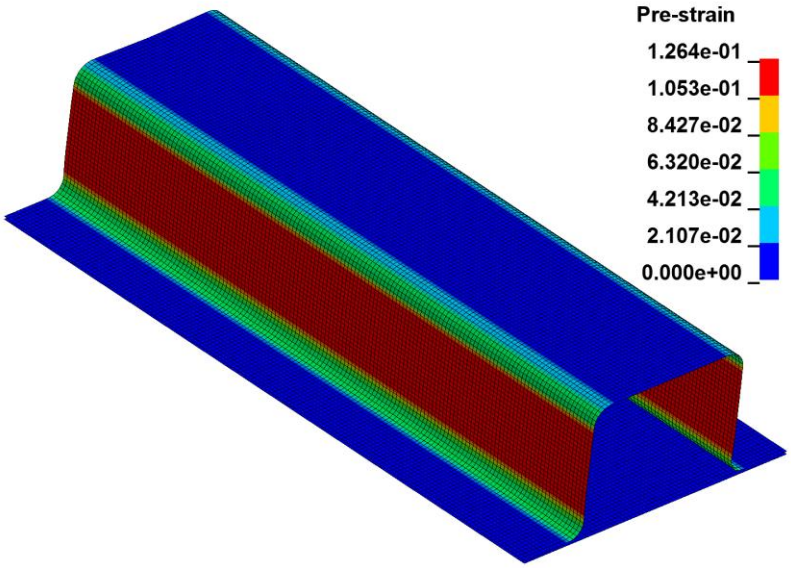

Fig.12: fringe plot of the pre-strain distribution on the part after springback.

The pre-strain in the formed component is only present in a significant way in the vertical sidewalls of the channel. This is a consequence of the bending and un-bending during drawing.
After the tube model has been prepared in such a way, the final axial crush simulations are executed. A rigid plate is used to crush the tube from one side while the other side is fully constrained using nodal constraints. The total plate displacement in the simulation was approximately 200 mm. Two cases were run in the axial crush simulation:

1. Pre-strain as calculated
2. Pre-strain set to zero

Since there is no experimental validation data available at this time, the aim of this exercise is to gauge the magnitude of influence on the simulation results of including vs. excluding the pre-strain dependent age-hardening response in the model.

5.3 Results

The tube geometries before and after the axial crush are shown for both cases on Fig. 13. The crushed geometry varies somewhat between the two cases, particularly in the second buckle. This might be caused by the fact that the only significant difference in strength is in the vertical sidewalls of the channel, where there is an accumulation of pre strain due to bending and un-bending, thus inducing a slightly different buckle mode.

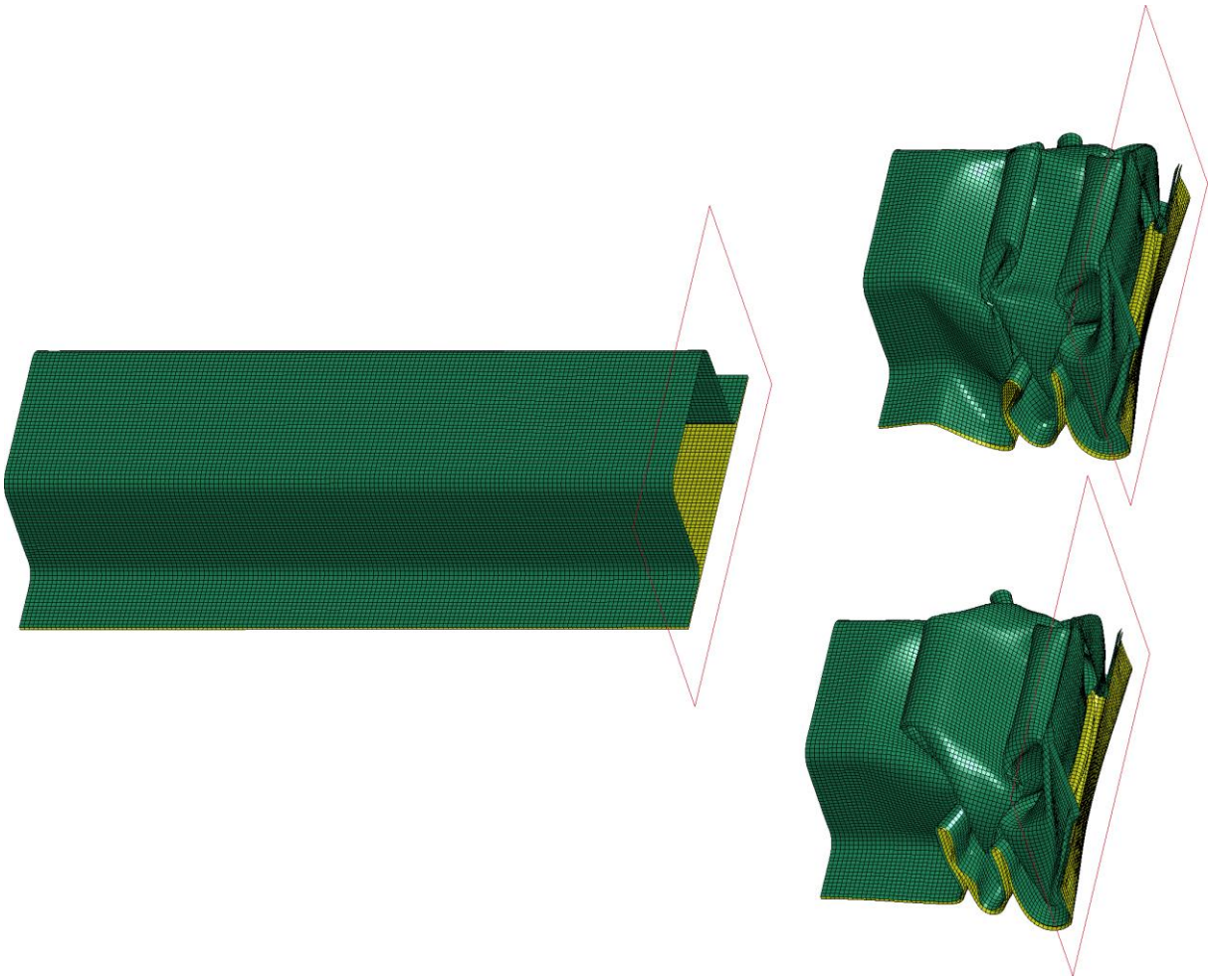

(a) (b)

Fig.13: top hat tube a) before crushing and b) at 200 mm plate displacement, with pre-strain top and without per-strain bottom.

The force-displacement response of the tube during axial crushing for both cases is shown on Fig. 14.

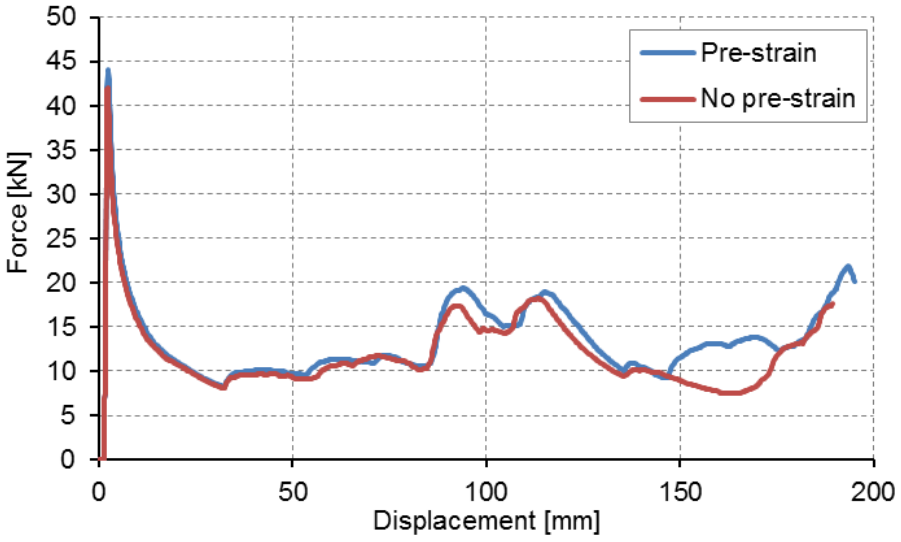

Fig.14: force-displacement response during axial crushing.

The case with pre-strain included shows a higher force across the range, although the differences are not very pronounced. The largest difference is present in the later stages of buckling, which coincides with the formation of the second buckle on the tube where, as stated above, the bucking modes differ.

Fig. 15 shows the energy absorption during buckling for both cases.

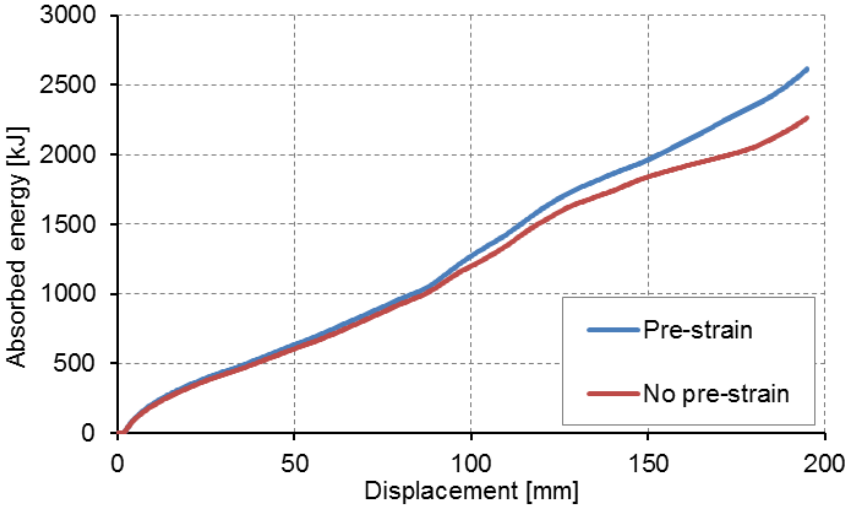

Fig.15: energy absorption during axial crushing.

Energy absorbed during axial crushing shows the differences between the two cases much more clearly. For the entire duration of the test, the case which includes pre-strain effects absorbs energy at a higher rate. The total energy absorption at the end of the test is 2.62 kJ with the pre-strains included and 2.26 kJ without, which is about a 16 % increase in energy absorption. The presented model; however, does not consider damage. Since the greatest differences occur later on in the crushing process, the benefits of the pre-strain effects might be much less pronounced if damage was present.

6 Summary

The yield stress prediction given by the microstructural model was successfully validated with the tensile test and cup draw test results. The accuracy of the prediction is within reasonable limits and allows for use of the predicted yielding behaviour in future numerical analysis which could greatly influence alloy design for crash applications. Yield stress in itself; however, is not sufficient as an input for material data in finite element simulation. For future work, implementation of a working hardening model which follows Kocks-Mecking theory [5,6] is considered to further expand the capabilities of the microstructural model in assisting finite element analysis.
The inclusion of pre-strain dependent paint-bake response in a component level buckling simulation has shown to significantly influence the final simulation results. Despite the simplistic implementation, the local increase in yield strength showed a marked increase in the energy absorbed by the component during axial crush. For more complex components where the strain distribution after forming is far more intricate, these effects are expected to be even more pronounced, which is of particular significance in automotive crash simulation. An expansion of the concept presented here is foreseen in future work to include pre-strain effects on the integration point level as well as coupling with thermal analysis to account for influence of heat treatment on the final component strength.

7 Literature

[1] J. Hirsch, Aluminium Alloy for Automotive Application, Material Science Forum, 242 (1997), pp. 33-50
[2] Deschamps A, Brechet Y. Influence of predeformation and ageing of an Al–Zn–Mg alloy—II. Modeling of precipitation kinetics and yield stress. Acta Materialia. 1998;47:293-305
[3] F. X. Mao, C. Bollmann, T. Brüggemann, Z. Q. Liang, H. C. Jiang, V. Mohles, "Modelling of the Age-Hardening Behavior in AA6xxx within a Through-Process Modelling Framework", Materials Science Forum, Vol. 877, pp. 640-646, 2017
[4] EN ISO 6892-1:2009: Metallic materials - Tensile testing - Part 1: Method of test at room temperature. 2009.
[5] L. M. Cheng et. al.: The Influence of Precipitation on the Work-Hardening Behavior of the Aluminum Alloys AA6111 and AA7030. Metall. Mater. Trans., Vol. 34A, 2003, pp. 2473
[6] A. Simar et. al.: Sequential modeling of local precipitation, strength and strain hardening in friction stir welds of an aluminum alloy 6005A-T6. Acta Mater. Vol. 55, 2007, pp. 6133-6143